Stochastic uncertainty quantification of seismic performance of complex large-scale structures using response spectrum method

Huidong Zhang[1,2*], Xinqun Zhu[3], Xiao Liang[1,2], Fuyan Guo[4]

[1]School of Civil Engineering, Tianjin Chengjian University, Tianjin 300384, China

[2]Tianjin Key Laboratory of Civil Buildings Protection and Reinforcement, Tianjin 300384, China

[3]School of Civil and Environmental Engineering, University of Technology Sydney, NSW 2007, Australia

[4]School of Control and Mechanical Engineering, Tianjin Chengjian University, Tianjin 300384, China

Abstract: Imprecision or uncertainty always exists in engineering structures. In recent years, an increasing emphasis is placed on quantifying structural performance by explicitly modeling uncertainties. A limited number of studies have been conducted on uncertain analysis of complex structures. The time history response analysis is extremely time-consuming to solve uncertain problems of complex structures. In this paper, a new probabilistic finite element method using response spectrum analysis has been developed to analyze the full-scale lattice dome structures with uncertain parameters. Based on the proposed method, the lattice dome structure under different earthquake intensity levels is investigated and the probabilistic structural demands are quantified. The results show that compared with the perfect dome, the mean deformations and reaction force values at the supports caused by earthquakes in the uncertain dome increase, the mean axial force values of the members decrease, and the structural demands present large uncertain intervals, indicating that the uncertain variables in the dome lead to an increase in the failure probability. The effect of uncertain error sources on the structural demands is discussed. This study provides possible applications for the probability-based performance analysis of super large-scale structures with uncertain parameters.

Key words: large-scale dome; uncertain parameter; probability analysis; seismic performance; response spectrum method.

1. Introduction

In recent decades, a number of surveys have been conducted on structural failures, and it is found that the causes of structural failures [1-4] are, with some exceptions, attributed to human errors. A series of investigations [5, 6] indicated that human errors in the structural design or construction are responsible for most of structural failures. Usually, incorrect model assumptions or insufficient considerations in material behaviors, loads and actions [7] are considered to be important human errors. Further investigations [8, 9] also showed that a large number of inadequate considerations occurred in structural analysis. Fig. 1 summarizes the proportion of causes of structural failures caused by human errors [8]. In Fig. 1, it is found that design and construction errors are the important causes of structural failures.

Ellingwood [2] pointed out that if there is no error control, structural safety is much likely to be affected by construction errors. Compared with perfect structures, construction errors lead to various types of uncertainties in a structure. In practice, structures are not perfect in many aspects, such as structural geometric imperfections. Imperfections in structural systems are inevitable and cannot be completely eliminated in construction process. When a structure is mainly subjected to compressive loads, geometric imperfections may become particularly dangerous because of the possibility of sudden collapse in the structure [10]. Furthermore, imperfections caused by human errors are characterized by randomness, and therefore these random imperfections should be considered in structural analysis.

*Corresponding author: Huidong Zhang, School of Civil Engineering, Tianjin Chengjian University, Tianjin 300384, China

E-mail: zhhuidong@126.com

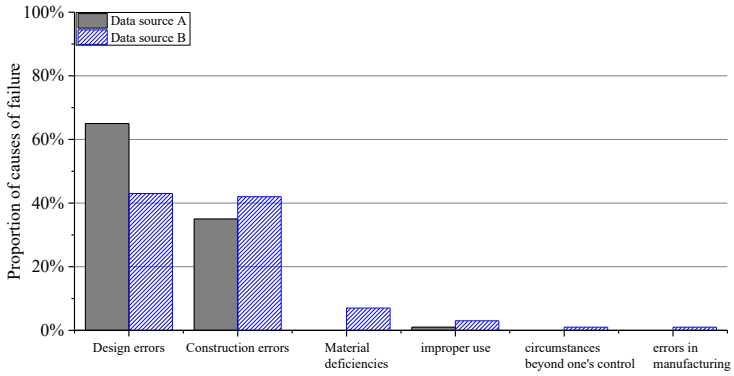

Fig. 1 Causes of structural failures [8]

The effects of geometric imperfections on the static stability of large-scale single-layer lattice domes have been extensively investigated [11-13]. In these studies, the linear or nonlinear bulking analysis (BA) methods were adopted by considering the worst imperfect shape, where an imperfection factor was usually assumed, and a Monte Carlo simulation was performed to consider the randomness of the imperfections. The random values of imperfections are controlled by the construction quality and human errors, and they vary within a range. Therefore, a deterministic structural analysis will not be sufficient to properly evaluate the structural performance. Moreover, many other uncertainties exist in structures, such as material parameters, section parameters, roof loads, and structural damping ratios, which are stochastic in the life cycle of a structure and have different degrees of impact on structural performance. All these aspects lead to uncertainties in a structural analysis model. However, significant simplifications have been made in deterministic models, and only the safety factors were used to consider the structural uncertainties.

In the seismic analysis of structures, it has been suggested [14] that uncertainties should be directly introduced into performance-based earthquake engineering (PBEE) research. More recently, the uncertain modeling of structures in PBEE research has begun to focus on the explicit consideration of uncertainties in many parameters, such as constitutive model parameters, shape imperfections, loads, damping, and ground motions, in which, as stated by Bradley [15], unlike those low-level constitutive model parameters, the uncertainties at the structure-level are at a high level and tend to focus on the specific problems and systems. Therefore, it is challenging to carry out uncertain numerical simulations and analyses for complex structures. The challenge is mainly reflected in two aspects: the complexity of numerical modeling and the time-consuming computation.

The assessment of uncertain structures plays an important role in PBEE. Probabilistic structural analysis offers the unique tool to analyze uncertainties in structural designs, while probabilistic evaluations for large-scale structures can only be realized by computer simulations [16], which help to improve performance predictions and solve structural reliability problems. Various computer-aided tools have been developed in structural engineering, and performance-based analysis has been a beneficiary.

Structural performance is commonly evaluated by time-history response analysis (THRA) and response spectrum analysis (RSA) methods [17]. The THRA method is time-consuming or even impossible when solving the probabilistic problems of uncertain structures, and it is unrealistic to use this method to analyze a large number of sampling structures with uncertain parameters, especially for super large-scale structures. At present, RSA is an important structural seismic analysis method and can approximately estimate the structural demands under transient dynamic loads in a quasi-static manner. In particular, it can solve the probabilistic problems of uncertain large-scale structures faster than

THRA method. In general, a limited number of studies have been performed for uncertain analysis problems under dynamic loading or quasi-static conditions, and they are only restricted to simple structures, such as the structures in the literature [17, 18]. Recently, a probabilistic assessment for three-dimensional frame structures under bidirectional seismic excitations was implemented using RSA with the complete quadratic combination (CQC) method [19]. According to the site response spectra, Moustafa and Mahadevan [20] developed a reliability analysis method for structures with uncertain parameters to avoid explicit dynamic analysis for three-dimensional structures. Generally, studies on complex uncertain structures are still limited.

The single-layer lattice domes are important typical public buildings. However, the probabilistic structural performance analyses for large-scale single-layer lattice domes with various types of uncertainties have not been extensively carried out in the PBEE framework because of the structural shape and complexity.

The key objectives of the paper are as follows:

- introduce the probabilistic analysis and RSA methods into a super large-scale single-layer lattice dome in PBEE methodology;
- provide modeling methods of important low-level and high-level sources of uncertainties by introducing stochastic fields in association with probability distributions and accounting for the intervals of the variables in a dome;
- develop a probabilistic finite element code to evaluate the structural performance using the RSA method based on the Abaqus and Python platforms; and
- determine the effects of the uncertain variables and analysis methods on structural failure.

2. Modeling methods for imperfect structures

2.1 Geometric imperfections

Usually, geometric imperfections in a steel structure include [10, 11]: (a) global structural shape imperfections, (b) member shape imperfections, and (c) cross-sectional imperfections.

(a) Global shape imperfections (structural level)

In the finite element method, the geometry Ω of the dome is described by a set of nodes $\{R_i, i = 1, \dots N\}$. A nodal deviation caused by geometric imperfection is shown in Fig. 2.

The deviation of each node can be represented by a random vector $\{\Delta R_i = \{\Delta X_i, \Delta Y_i, \Delta Z_i\}, i = 1, \dots N\}$, and each component in ΔR_i is random, which can be described by a probability density function (PDF). The relationship between the design position of a node $\{R_i\}$ and its real position $\{R_i'\}$ can be described by the following equation,

$$\{R_i'\} = \{R_i\} + \{\Delta R_i\} \tag{1}$$

For a given node, the nodal deviation value $Err(\Omega_i)$ is computed by the following equation,

$$Err(\Omega_i) = \sqrt{\Delta X_i{}^2 + \Delta Y_i{}^2 + \Delta Z_i{}^2} \tag{2}$$

where ΔX_i, ΔY_i, and ΔZ_i are the coordinate deviations of a node in the x, y, and z directions, respectively. This method has been used for uncertain analysis in the literature [14].

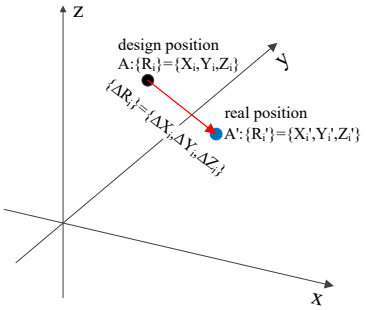

Fig. 2 Node deviation in three-dimensional space.

The imperfection amplitude refers to the maximum node deviation from the design position. However, the nodal imperfection amplitude is bounded because of error control. For example, for a node with an imperfection amplitude d_{max}, assuming that each component in ΔR_i has the same probability distribution and bound, then each component has a maximum deviation value of $d_{max}/\sqrt{3}$ according to Eq. (2). Thus, each component is within the range,

$$-d_{max}/\sqrt{3} \le [\Delta X_i, \Delta Y_i, \Delta Z_i\,] \le d_{max}/\sqrt{3} \tag{3}$$

For a large-span steel dome, according to the investigation findings, the imperfection amplitude of each component is equal to $min\{L/1500\ m, 0.04\ m\}$ [21], where L is the span length of the dome. In addition, it was also reported that the approximate imperfection amplitude of each component in ΔR_i should be set to $L/500\ m$ [22]. According to the field tests for a large-scale dome [23], the node deviation amplitude of each component is approximately 0.03 m, the standard deviation is near 0.0173 m, and the distribution of the node deviation is close to a normal distribution.

A Monte Carlo simulation (MCS) is performed and a series of nodes with errors are randomly generated, as shown in Fig. 3. Here, the node error of each component has a Gaussian distribution with a mean of zero, standard deviation of 0.0231 m, and bound ranging from {-0.0693 m, 0.0693 m}. Each actual nodal position of an imperfect dome is within a sphere with the ideal node position as the sphere center.

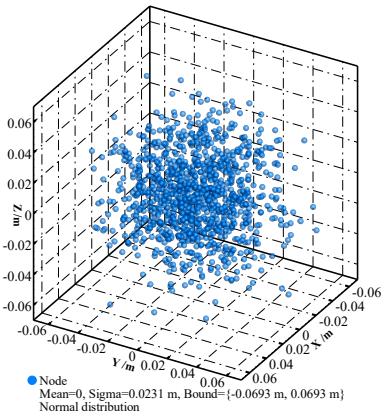

Fig. 3 Node deviations for one sample

(b) Member imperfections (member level)

Initial geometric imperfections include local and overall imperfections [12]. Initial local geometric imperfections refer to the surface imperfections of steel members. The initial overall geometric imperfection is the profile imperfection of the whole member along the member length, whose direction is random. In this paper, only the overall geometric imperfection is considered. Here, the initial overall member imperfection considers the initial deflection of the member, residual stresses, and initial eccentricity of the member. The initial deflection $\omega_1(x')$ of a member, the deflection $\omega_2(x')$

caused by residual stresses, and the deflection $\omega_3(x')$ caused by the initial eccentricity produce a total equivalent imperfection $\omega(x')$, as shown in Fig. 4.

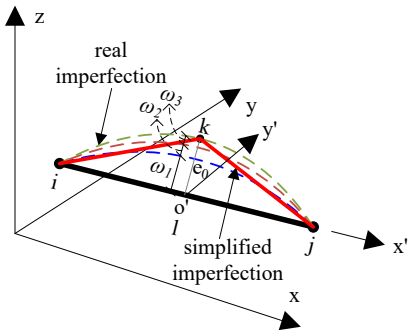

Fig. 4 Member imperfections

In Fig. 4, the total equivalent imperfection can be written as,

$$\omega(x') = \omega_1(x') + \omega_2(x') + \omega_3(x') \tag{4}$$

Usually, the imperfection of a member with a length l is described by a half wave shape [11],

$$\omega(x') = e_0 \, sin\left(\pi x'/_l\right) \tag{5}$$

where e_0 is the deflection at the mid-span. In this paper, an additional node k with a node deviation of e_0 in the direction perpendicular to the member is added to simulate the imperfection. Here, e_0 is a variable that has a given probability distribution. Because node k is located in a plane perpendicular to the x' axis, the node deviation of each component is within a circular area, and each component is bounded in the following range,

$$-e/\sqrt{2} \le [\Delta y_i', \Delta z_i'] \le e/\sqrt{2} \tag{6}$$

where $\Delta y_i'$ and $\Delta z_i'$ are the node deviations in the local $x'o'y'$ coordinate system. Here, the node deviation $\Delta x_i'$ is equal to zero. Then, the node deviations are converted to the global coordinate system. For global imperfections, typically, 1/1000 of the span length is used as the imperfection magnitude e_0 [24]. The imperfections will not lead to initial forces or structural stresses. In this paper, the member imperfection was explicitly modeled in finite element simulation.

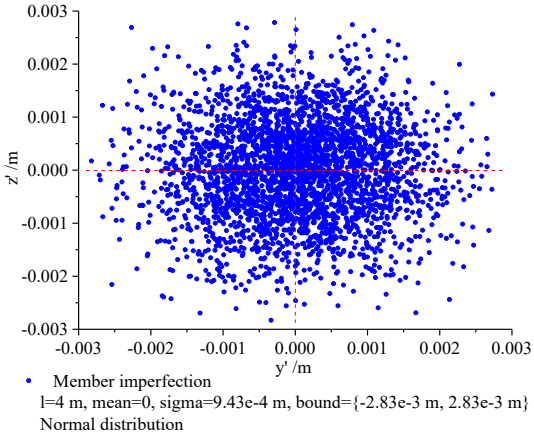

Fig. 5 Member imperfection for one sample

Here, an MCS simulation is performed, and the imperfection errors of a series of members are generated for the y′ and z′ directions, as shown in Fig. 5. The imperfection error of each component has a Gaussian distribution with a mean of zero. Here, a given member length is l=4 m, the imperfection amplitude is set to be l/1414 for the y′ and z′ directions, and the standard deviation is set to be

l/(1414*3). The imperfection errors are within a circular area with a radius of $r_a = l/1414$. This means that each actual nodal position of the mid-span node in an imperfect member is within a circular area with an ideal node position as the circle center, and the circular area is perpendicular to the member. In current study, the length of each member is automatically calculated according to the nodal coordinates with deviations.

(c) Cross-sectional imperfections (section)

Cross-sectional imperfections refer to the change of the ideal cross-sectional shape [12]. The most common approach to describe cross-sectional imperfections is to consider the cross-section thickness as a variable [25]. A series of detailed measurements for cross-section thickness of steel pipes and continuous metal shells have been reported [12, 26], and it was observed that the distribution of thickness was generally symmetric and could be approximately characterized by a Gaussian probability density function; the standard deviation of the wall thickness is approximately 280 μm; however, the wall thickness typically has a magnitude of ± 1 mm. The imperfection errors can also be generated using the MCS method. In addition, local imperfections for cross-sections are not considered in this paper.

2.2 Other important parameters

The elastic modulus of steel material is also of particular interest to structural engineers. Structural stability also relies on this parameter. Based on the material experiments, a significant variability in the elastic modulus has been found for steel material [27]. According to a series of experimental studies on the elastic modulus [27], the elastic modulus E can be best described by a normal distribution with a variation factor of 0.045.

In deterministic analysis, roof load is typically considered to be uniformly distributed. In reality, roof load varies spatially in the life cycle of a structure according to expert surveys. The roof load can be appropriately modeled by the PDF of a Gaussian distribution [28], and it is also observed that the roof load value has a bound, which is neither arbitrarily large nor arbitrarily small. Many codes suggest [29-31] that a standard deviation factor of 0.2 to 0.3 is appropriate. However, more detailed information is lacking for roof loads.

For structures subjected to earthquake ground motions, more uncertainties result from damping, which includes the uncertainties coming from the damping mechanism and damping ratio. This study does not consider the uncertainty coming from the damping mechanism and assumes the viscous damping mechanism. The quantification of the damping ratio in a structure depends on many factors, such as identification methods and estimation technologies, leading to large variability [32]. It was observed that the variability in damping was as high as between 30% and 80%, and generally, the damping ratios tend to follow a log-normal distribution [33]. Nevertheless, a simple single PDF may not well describe the distribution of structural damping ratios. In this study, a complex distribution is assumed and introduced to present the uncertain characteristics of damping ratios. Here, it is assumed that the mean values of the modal damping ratios follow a Gaussian distribution, and then the damping ratios with this mean value follow a logarithmic normal distribution, as shown in Eq. (7)

$$\begin{cases} \xi_0 \sim N(\mu, \sigma^2) \\ \mu \sim LN(mu(\xi_0), [sigma(\sigma)]^2) \end{cases} \tag{7}$$

where ξ_0 is the mean value of the damping ratios, μ is the mean value of ξ_0, σ is the standard deviation of the damping ratios, $mu(\xi_0)$ is the mean value of the logarithmic values, and sigma(σ) is the standard deviation of the logarithmic values. A comparison between the normal distribution and the normal-lognormal distributions for the damping ratio is performed using the MCS method, and the

sample size is 10000, as shown in Fig. 6. Here, the damping ratios have a bound of $\{0.01, 0.05\}$, a mean value of 0.03, and a standard deviation of 0.01. It is observed that the damping ratios following the normal and lognormal distributions are more discrete than those following only the normal distribution, and the probability of obtaining the maximum or minimum damping ratio increases in the normal and lognormal distributions, presenting a complex characteristic.

Unlike the node deviations and the member imperfections, for the above variables, their uncertainties are assigned to the overall structure based on the sampling in this study.

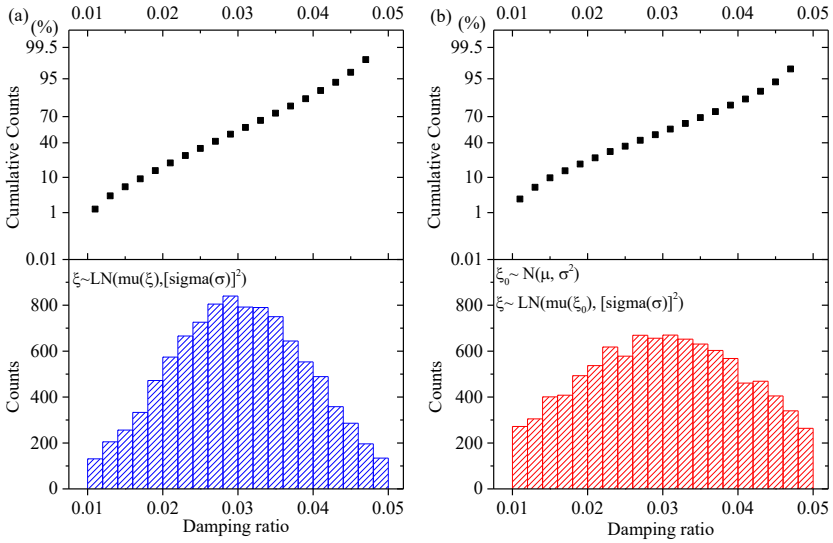

Fig. 6 Comparison between the lognormal distribution and the normal and lognormal distributions

3. Numerical example

3.1 Model and uncertain parameters

A welded Kiewitt8 (K8) large-scale single-layer lattice dome [34] is selected as an example. The model is shown in Fig. 7 (a). Steel pipes have a cross-section with a size of ϕ146×5 mm. The uniform roof load is 150 kg/m^2. The additional information can be found in the literature [34].

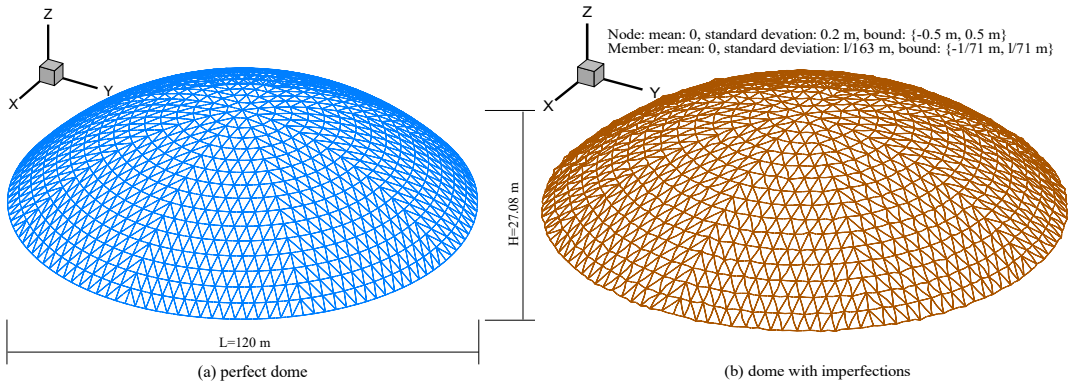

Fig. 7 Perfect dome [34] and dome with imperfections

A 3-dimensional numerical model of the perfect dome was established in Abaqus. The steel members were modeled using beam element B31. An elastic-perfectly plastic steel material model was used in the study. The finite element model consists of 4225 nodes and 6272 elements. A sample dome with shape imperfections and member imperfections is presented in Fig. 7(b). It should be noted that to better present the dome with imperfections, larger values are used for the standard deviations and bounds of the imperfections. In RSA method, the CQC method is selected in the structural analysis, and

the responses under the multidirectional excitations are combined using the 40% rule [35]. The literature [35] provides more details for the RSA method.

According to the previous analysis, the important variables in a dome are listed in Table 1. Each variable is bounded within a range. All these values listed in Table 1 are based on the literature listed above and related codes. Unlike the study in the literature [14], all these variables are explicitly modeled in current study.

Table 1 Variables in the uncertain structure

Variable (V)		Bound	Mean	Standard deviation (σ)	Distribution
Elastic modulus /Pa		{1.9e11, 2.22e11}	2.06e11	9.27e9	$V \sim N(mean, \sigma^2)$
Node deviation /m		{-0.069, 0.069}	0	0.0231	
Member imperfection /m		{-l/1414, l/1414}	0	l/4242	
Cross section thickness /mm		{-1, 1}	0.005	0.28	
Roof load /kg		{1620, 1980}	1800	133.2	
Damping	μ	{0.01, 0.05}	0.03	0.01	$V \sim N(mean, \sigma^2)$
	Damping ratio	{0.01, 0.05}	μ	0.01	$\boldsymbol{V \sim LN(\mu, \sigma^2)}$

3.2 Development of a probabilistic finite element code

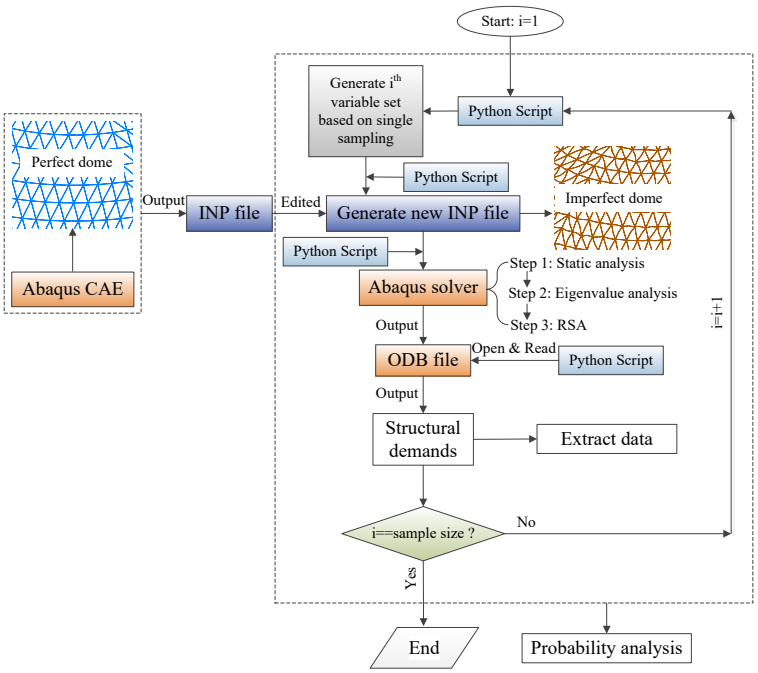

Fig. 8 Computing procedure for uncertain analysis

The analysis of the uncertain structure is carried out in Abaqus ©v6.14.4 and Python ©v3.6. To run the simulation, the perfect model is first created and meshed in the Abaqus CAE and then saved. After the INP file for the perfect model is output, based on the Python scripts coded in the Python environment, a group of variables are generated using the MCS method according to Table 1. The perfect positions of the individual nodes are replaced by the imperfect node positions, and other variables are also assigned to the imperfect dome through Python scripts; thus, a new INP file for uncertain analysis is generated. The new INP file is submitted to the Abaqus solver, and the Abaqus solver is invoked by the Python scripts to solve the dynamic demands and generate the ODB file. Then, the ODB file is opened and read using Python scripts; thus, the structural demands are extracted. The

computations stop once the sample size is reached. Here, probability analysis is performed using MATLAB software based on the extracted data. This computing procedure is presented in Fig. 8.

In this study, the computations are carried out on a single Intel(R) Xeon(R), 3.50 GHz CPU with 32 GB of RAM memory. The total computation time taken to solve the structural demands per 5000 sample structures is approximately 61.7 hours.

It has been found that the THRA method [14] can only carry out structural probability analysis with a small number of ground motions, and the sampling size cannot be very large, otherwise, the structural analysis cannot be run. Compared with the THRA method, the RSA that avoids the explicit dynamic analysis of the uncertain structures is a quasi-static analysis method and can be directly used for larger scale computations with a higher sampling precision.

3.3 Sample size

In the MCS, the solution converges as the sample size increases. An accurate solution can be obtained by using a sufficiently large sample size. However, the computational cost increases with the increase in sample size. For the variables with bound ranges, the required sampling size is far less than that required in an ordinary MCS. The convergence criteria have been proposed and verified in the literature [14], where only a relatively small sampling size with the order of magnitude of 1×10^3 can make the solution converge. According to this method, a sampling size of 5000 is selected for each analysis in this paper. The sampling size is sufficient to perform the probability structural analysis. In this paper, although the direct MCS is used, it may obtain the accurate results in engineering, while those improved MCS methods may get accurate results in mathematics because the PDFs of the uncertain parameters used in an analysis were fitted based on the previous limited test data. In addition, due to the spectacular growth of computing capacity at present, it is not difficult to calculate the structural demands of 5000 uncertain structures.

3.4 Dynamic characteristics of the dome

The first 150 mode frequencies of the perfect dome and two sample domes with the parameters in Table 1 are shown in Fig. 9. The frequencies generally increase linearly, and the uncertain variables of the dome have an obvious effect on the frequencies. The first frequencies of the three domes are 1.4051 Hz, 1.254 Hz, and 1.3318 Hz, respectively.

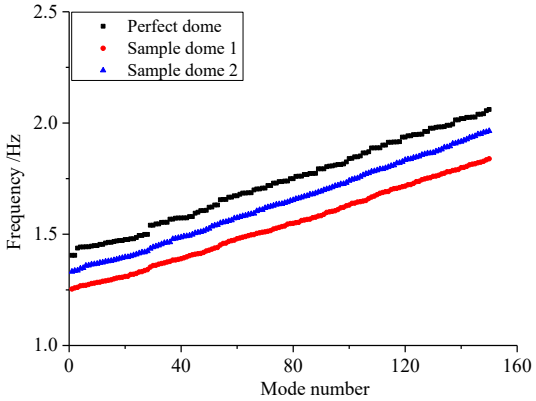

Fig. 9 Frequencies of the domes

The total response of the dome is equal to the superposition of each mode, and it is usually not necessary to include all high-order modes in the superposition process because the modes with the lower frequencies generally have the larger effect on the structural demands, while the effect of the higher-order modes tends to decrease. In this study, the first 150 modes are used to estimate the structural demands. Although the total effective mass of the 150 modes covers approximately 85% of

the total structural mass, for complex structures, the accuracy of the calculation for higher order modes using the finite element method is relatively low, and it is necessary to limit the number of vibration modes that are considered in RSA.

The distributions of the 1st and 20th frequencies from 5000 sampling structures are shown in Fig. 10. The frequency values of the 1st and 20th modes range from approximately 1.1 Hz to 1.55 Hz and from 1.2 Hz to 1.65 Hz, respectively. The mean frequencies are 1.357 Hz and 1.426 Hz for the 1st and 20th modes, respectively. For the perfect dome, the frequencies are 1.4051 Hz and 1.4759 Hz, respectively. The differences between the perfect dome and the sample dome are caused by the uncertain parameters in the sample structure. Overall, the distributions seem to be approximately normal.

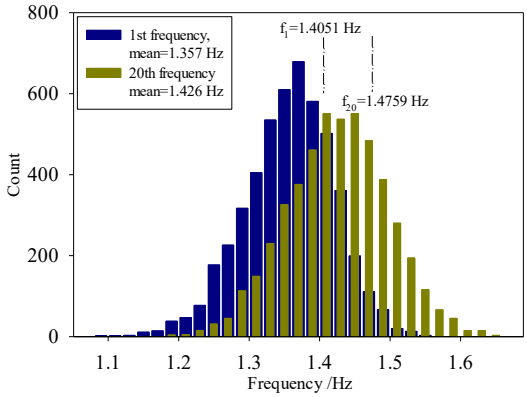

Fig. 10 Frequency values of the 1st and 20th modes of the sample dome

3.5 Earthquake ground motions

As listed in Table 2, 10 natural seismic records are selected from the literature [17, 20] for the structural analysis. According to the information, the spectra can be plotted according to the acceleration data from the PEER Strong Ground Motion Databases. Fig. 11 shows the acceleration spectra and the mean spectra of these ground motions.

Table 2 Earthquake ground motions [17, 20]

Year	Event	Recording station	Mw	Fault distance /km
1979	Imperial Valley-06	Chihuahua	6.5	7.3
1976	Gazli, USSR	Karakyr	6.8	5.5
1980	Irpinia, Italy-01	Calitri	6.9	17.6
1983	Coalinga-01	Pleasant Valley P.P bldg	6.4	8.4
1986	N. Palm Springs	Whitewater Trout Farm	6.1	6.0
1989	Loma Prieta	BRAN	6.9	10.7
1992	Cape Mendocino	Cape Mendocino	7.0	6.9
1994	Northridge	Pacoima Kagel Canyon	6.7	7.3
1999	Chi-Chi, Taiwan	TCU067	7.6	0.6
2002	Denali, Alaska	TAPS Pump Station #10	7.9	2.7

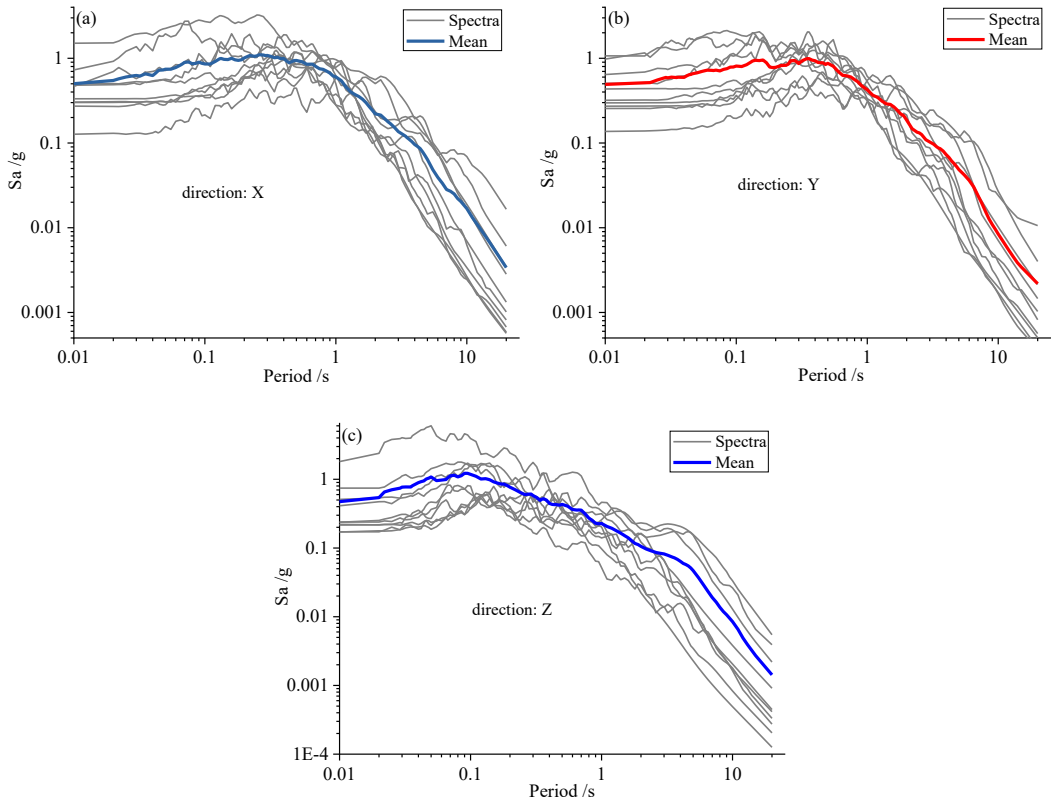

Fig. 11 Spectra of the natural earthquake ground motions

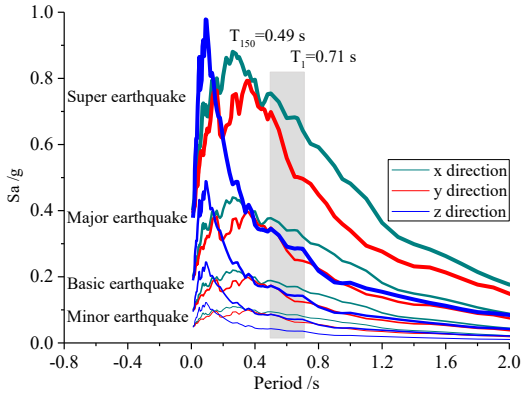

Fig. 12 Spectra for the uncertain analysis

The mean spectra in Fig. 11 are used in the RSA, which are adjusted by using scaled factors to construct the minor, basic, major, and super earthquakes. Based on minor earthquakes, the scaled factors are 2.0 for basic earthquakes, 4.0 for major earthquakes, and 8.0 for super earthquakes. The spectra that are used for the uncertain analysis are shown in Fig. 12. According to the eigenvalue analysis, the periods of the perfect dome fall approximately within the range of T_{150}=0.49 s to T_1=0.71 s.

3.6 Limit state

In a large-scale dome, the failure of the whole structure is often characterized by sudden collapse, which involves the safety of the whole structure. When a dome collapses, it can no longer withstand external loads. A nonlinear bulking analysis that is different from the traditional pushdown analysis method [14] is performed to determine the limit states of the dome in current study, and it takes into account the effects of horizontal seismic force on vertical deformation of the structure using scale

factors. It includes two analysis steps: (1) Linear eigenvalue buckling analysis: the structural failure modes under three-dimensional ground motions are considered, where static loads are first applied to each node in three directions, and the load scaling factors of the three directions are approximately 1, 0.85, and -0.5 (negative Z-axis), respectively, because it is observed in Fig. 12 that the scale factors of the spectrum values with periods of 0.49 s to 0.71 s are approximately 1, 0.85, and 0.5 for the X, Y, and Z directions, respectively; and (2) Post-buckling analysis: it is realized by means of static analysis using the Riks algorithm on the basis of the first step.

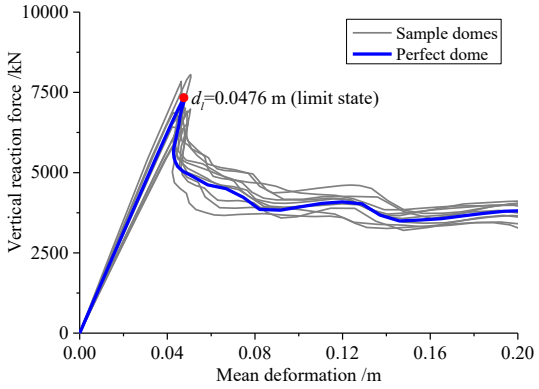

Fig. 13 Load-deformation curves.

Here, a statistical global deformation for the dome is adopted to determine the limit state using load-deformation curve. The statistical deformation of the dome is quantified by,

$$\Delta = \sqrt{\sum_{i=1}^{n} \Delta_i^2 / n} \tag{8}$$

where Δ and Δ_i are the mean vertical deformation of the dome and the vertical deformation of the i^{th} node, respectively; n is the number of nodes in the dome. According to the above analysis, the load-deformation relationships of the perfect dome and 10 sample domes are shown in Fig. 13. It is observed that the global deformation first increases linearly as the applied loads increase, and then when a critical deformation is reached, the total reaction force at the supports suddenly decreases, the dome loses stability, and its deformation continues to increase. The load-deformation curve of the perfect dome is close to the average level of the load-deformation curves of the sample domes. Therefore, in this study, the critical deformation d_l of the perfect dome is determined as the ultimate limit state.

However, it should be noted that the RSA involves the calculation of only the peak values of the structural demands. Here, statistically, it is assumed that the peak response of each node occurs at the same time for the RSA [20].

4. Structural probabilistic analysis

4.1 Distribution of the mean vertical deformation and the cumulative probability

According to the above analysis, when the vertical mean deformation d_l of the dome with uncertain parameters is reached, the structure is considered to be out of service. The structural safety can be described by the cumulative probability curve. The cumulative probability represents the probability value that is less than or equal to a displacement limit,

$$p_d = P(d \le d_l) \tag{9}$$

where d and d_l are the mean vertical displacement and displacement limit, p_d is the probability value when $d \le d_l$, and $P(\cdot)$ is the cumulative probability function of the displacement d. Here, the statistical vertical mean displacement d_i of the i^{th} sample structure is statistically determined by the following equation,

$$d_i = \sqrt{\sum_{i=1}^{n} \Delta_i^2 / n} \quad (10)$$

The cumulative probability curves of the sample structures under minor, basic, major, and super earthquakes are shown in Fig. 14. Each cumulative probability curve in Fig. 14 is obtained based on 5000 sample structures. According to Fig. 14, it is observed that the probability p_d of the displacement being less than d_l=0.0476 m is 100% under minor, basic, and major earthquakes. This indicates that the dome with uncertain parameters will not fail under these earthquakes, and the structure is sufficiently safe. However, under the super earthquake, the probability p_d of the displacement being less than d_l=0.0476 m is only 0.72%, while the probability of the displacement being larger than d_l=0.0476 m will be as high as 99.28%. Clearly, this structure fails in a super earthquake with a very high probability.

For the perfect dome, the mean vertical displacements are 0.065 m, 0.013 m, 0.0259 m, and 0.0522 m under minor, basic, major, and super earthquakes, respectively. According to the 5000 sample structures, the mean vertical displacement values of the imperfect dome are 0.0066 m, 0.0133 m, 0.0265 m, and 0.0531 m, respectively. Compared with the perfect dome, the mean vertical displacement values of the imperfect dome are slightly larger than those of the perfect dome. Moreover, they have uncertain intervals of {0.0056 m, 0.0082 m}, {0.0111 m, 0.01644 m}, {0.0222 m, 0.0329 m}, and {0.0445 m, 0.0657 m}. Clearly, they are not deterministic, and these values lead to the variation in estimating the displacement.

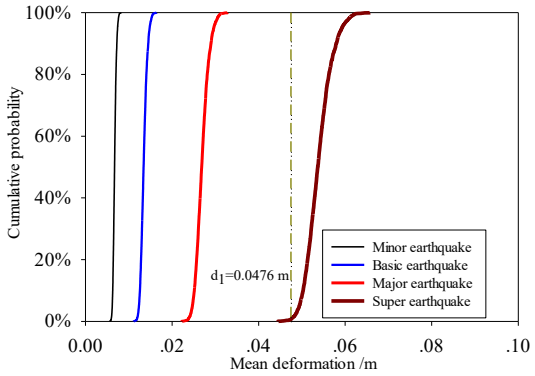

Fig. 14 Cumulative probability of the mean deformations

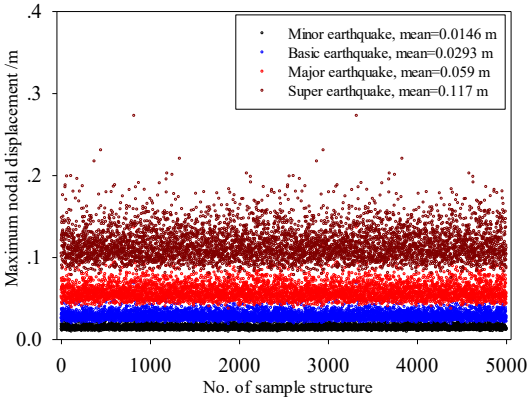

Fig. 15 Maximum vertical nodal displacement

Fig. 15 shows the maximum vertical nodal displacement values of each sample structure under the above earthquakes. Their mean values are 0.0146 m, 0.0293 m, 0.059 m, and 0.117 m, while these values are 0.0096 m, 0.0191 m, 0.0382 m, and 0.0764 m for the perfect dome, respectively, indicating that the uncertainties of the parameters greatly increase the structural deformation demand. Because the RSA is linear, these values also increase approximately linearly. Under the super earthquake, the maximum value of the nodal displacements in Fig. 15 is as high as 0.273 m, which is approximately 1/440 of the span length, while the maximum values of the nodal displacements under minor, basic, and major earthquakes are 0.0341 m, 0.0682 m, and 0.1364 m, respectively. The maximum displacement values also increase approximately linearly.

The cumulative probability distribution functions can be obtained by fitting the curves using the generalized extreme value (GEV) distribution with shape parameter k, scale parameter σ, and location parameter μ. The cumulative distribution function of the GEV distribution can be described by the following equation [36],

$$F(x;\ \mu, \sigma, k) = exp\ \{-[1 + k(\frac{x-\mu}{\sigma})]^{-1/k}\} \quad (11)$$

where x is the variable. The fitting curves for the four earthquake intensity levels are shown in Fig. 16. The shape parameters in the GEV distributions are very close, and they have a mean value of -0.1676, while the scale parameters and location parameters linearly increase as the earthquake intensity increases. It is also observed that if the parameters k, σ, and μ in the cumulative probability distribution function for the minor earthquake can be obtained, the parameters under other earthquake intensity levels are k, 2σ, and 2μ for basic earthquake, k, 4σ, and 4μ for major earthquake, and k, 8σ, and 8μ for super earthquake, respectively, and the parameters σ and μ depend on the earthquake intensity when using the RSA method. Thus, the cumulative probability distributions for different earthquake intensity levels can be predicted using those parameters under minor earthquake.

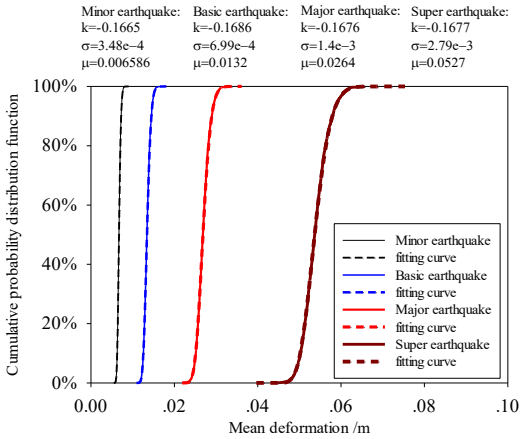

Fig. 16 Cumulative probability distribution functions of the mean deformation.

4.2 Distribution of the total vertical reaction force caused by earthquakes

Based on 5000 sample structures, the distributions of the total vertical reaction force (not including the gravity load) at the supports caused by the above four earthquake levels are shown in Fig. 17. Here, it is assumed that the peak vertical reaction force of each support occurs at the same time. The mean values of the total vertical reaction force caused by the earthquakes are 619 kN, 1237.7 kN, 2475.4 kN, and 4950.8 kN, respectively, while the total vertical reaction force values of the perfect dome are 614.9 kN, 1229.7 kN, 2460 kN, and 4918.8 kN, respectively. The vertical reaction force values for the imperfect dome are slightly larger than those of the perfect structure. In Fig. 17, the standard deviations increase linearly as the earthquake intensity increases. Therefore, according to the above analysis, this method can conveniently and approximately evaluate the seismic performance of imperfect domes under other earthquake levels based on a minor earthquake. For all cases, the variation coefficient (sigma/mean) of the vertical reaction force is approximately 0.0604. However, the uncertain structure causes a wide interval in the vertical reaction force. The intervals of the vertical reaction force are {492.02 kN, 723.4 kN}, {984.1 kN, 1446.5 kN}, {1968.2 kN, 2892.9 kN}, and {3936.4 kN, 5785.9 kN}, respectively. These intervals represent the uncertainties in the reaction force.

Fig. 18 shows the cumulative probability distribution curves and their fitting curves under the four earthquake levels. Among the distribution parameters in the fitting curves, the values of the shape parameter k are also very close and are approximately equal to -0.3, while the scale parameter σ and location parameter μ increase linearly, which depends on the earthquake intensity. Based on this, the distributions of the vertical reaction forces under other earthquake intensity levels can also be estimated using the data for minor earthquake in RSA.

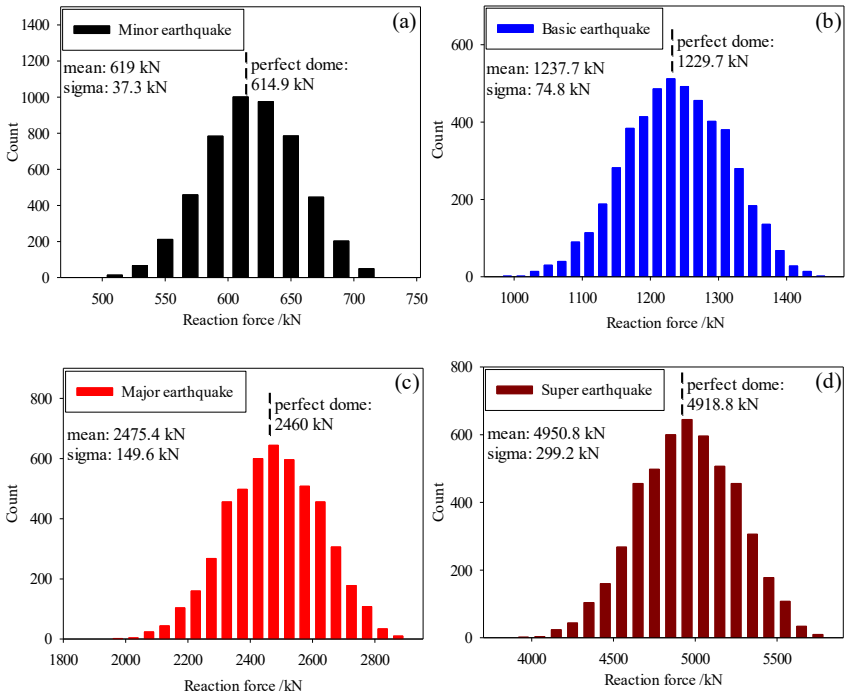

Fig. 17 Distribution of the vertical reaction force

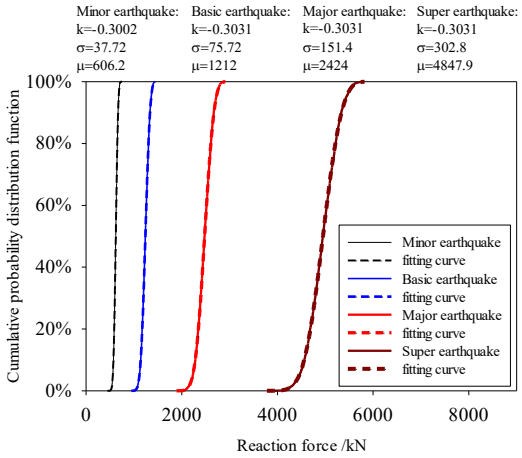

Fig. 18 Cumulative probability distribution function of the vertical reaction force

4.3 Vertical reaction force and vertical mean deformation

For each earthquake intensity level, the relationship between the total vertical reaction force and statistical vertical mean deformation is presented in Fig. 19. As the earthquake intensity level increases, the forces and deformations linearly increase within a radial interval and are uncertain but bounded. The degree of the data discretization depends on the earthquake intensity; that is, the greater the earthquake intensity, the more the force-deformation relationship deviates from the average curve. This indicates that the uncertainties of the structural performance increase with increasing earthquake intensity. Clearly, the uncertainties in a structure are an important factor that affects the structural performance, and they must be considered when estimating the structural demands. However, because the RSA method is linear, it is difficult to accurately predict the structural performance when a structure is highly nonlinear, such as when the mean structural deformation is larger than the limit deformation of 0.0476 m.

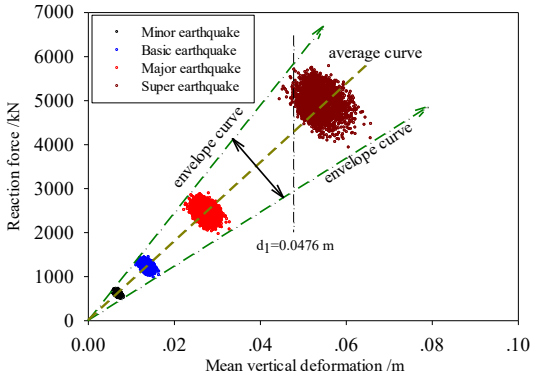

Fig. 19 Distribution of the relationship between the vertical reaction force and vertical mean deformation.

4.4 Axial force distribution due to an earthquake

Uncertainties in a structure result in uncertain axial forces in the members. The following index is used to describe the statistical mean axial force of a sample structure,

$$F_i = \sqrt{\sum_{i=1}^{n_e} F_{a,i}^2 / n_e} \tag{12}$$

where F_i is the statistical mean value of the axial force of all members in the i^{th} sample structure; $F_{a,i}$ is the axial force of the i^{th} element in the dome; and n_e is the number of elements of the dome.

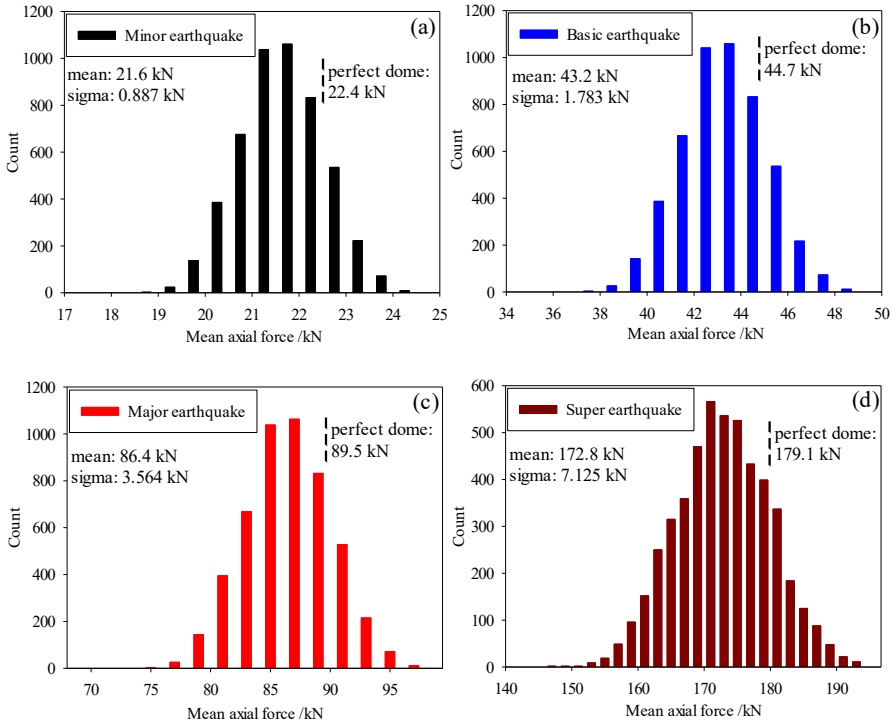

Fig. 20 Mean axial force distribution in the members.

Fig. 20 shows the distributions of the statistical mean axial forces of all members under minor, basic, major, and super earthquakes, in which the intervals of the mean axial forces are {18.4 kN, 24.2 kN}, {36.8 kN, 48.4 kN}, {73.6 kN, 96.7 kN}, and {147.2 kN, 193.3 kN}, respectively. The distributions in the statistics are approximately normal. The mean axial force values caused by earthquakes are 21.6 kN, 43.2 kN, 86.4 kN, and 172.8 kN, respectively, and they increase linearly. The standard deviations also increase linearly. Statistically, they have a variation coefficient of 0.041. In a perfect dome, the mean values of the axial force are 22.4 kN, 44.7 kN, 89.5 kN, and 179.1 kN. They are slightly larger than the

values of the dome with uncertain parameters. This is because the existence of uncertain parameters leads to a decrease in the overall stiffness of the structure.

The maximum axial force values in the domes with uncertain parameters are shown in Fig. 21. These values are also bounded, and they have mean values of 45.4 kN, 90.8 kN, 181.7 kN, and 363.4 kN. These data are not deterministic and have randomly distributed characteristics. Compared with the deterministic method, uncertain analysis can present uncertainties in the axial force. Although the calculation is time-consuming, the uncertain analysis of the structure has many advantages in engineering design.

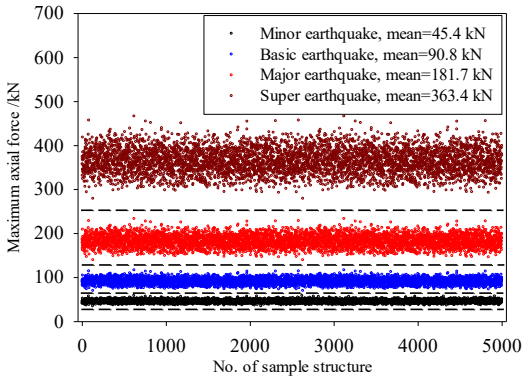

Fig. 21 Maximum axial force value in the dome with uncertain parameters.

4.5 Effect of the modal combination method on the structural demands

Some methods for performing the combination of peak modal responses are available. Typically, these methods are the square root of the sum of the squares (SRSS) method and the CQC method. In general, when the frequency difference between two adjacent modes is more than 20%, the effect of the cross-modal correlation is slight, and the results provided by CQC and SRSS methods are the same [37]. In this paper, the difference between the SRSS method and the CQC method in obtaining the peak modal demands is compared.

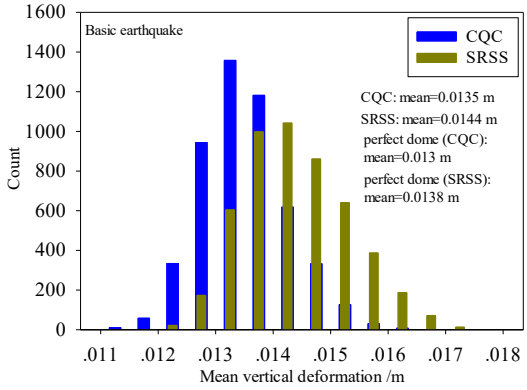

Fig. 22 Distributions of the mean vertical deformations using different combination methods.

Fig. 22 shows the distributions of the mean vertical deformations of the whole structure under basic earthquake using different combination methods based on 5000 sample structures. The mean values of the structural demands are 0.0135 m for the CQC method and 0.0144 m for the SRSS method. For the perfect dome, the mean vertical deformations of the whole structure are 0.013 m for the CQC method and 0.0138 m for the SRSS method. The cumulative probability curves of the mean vertical deformations, mean axial forces, and vertical reaction forces at the supports are shown in Fig. 23. Compared with the CQC method, the SRSS method is not conservative in estimating the deformation

demand of the uncertain dome; however, it is conservative in estimating the mean axial force and vertical reaction force caused by earthquakes. Especially in estimating the vertical reaction force, the two methods have a very large difference. Generally, the SRSS method does not yield appropriate results where the frequencies of the dominant modes of the structure are very close, such as for the dome structure.

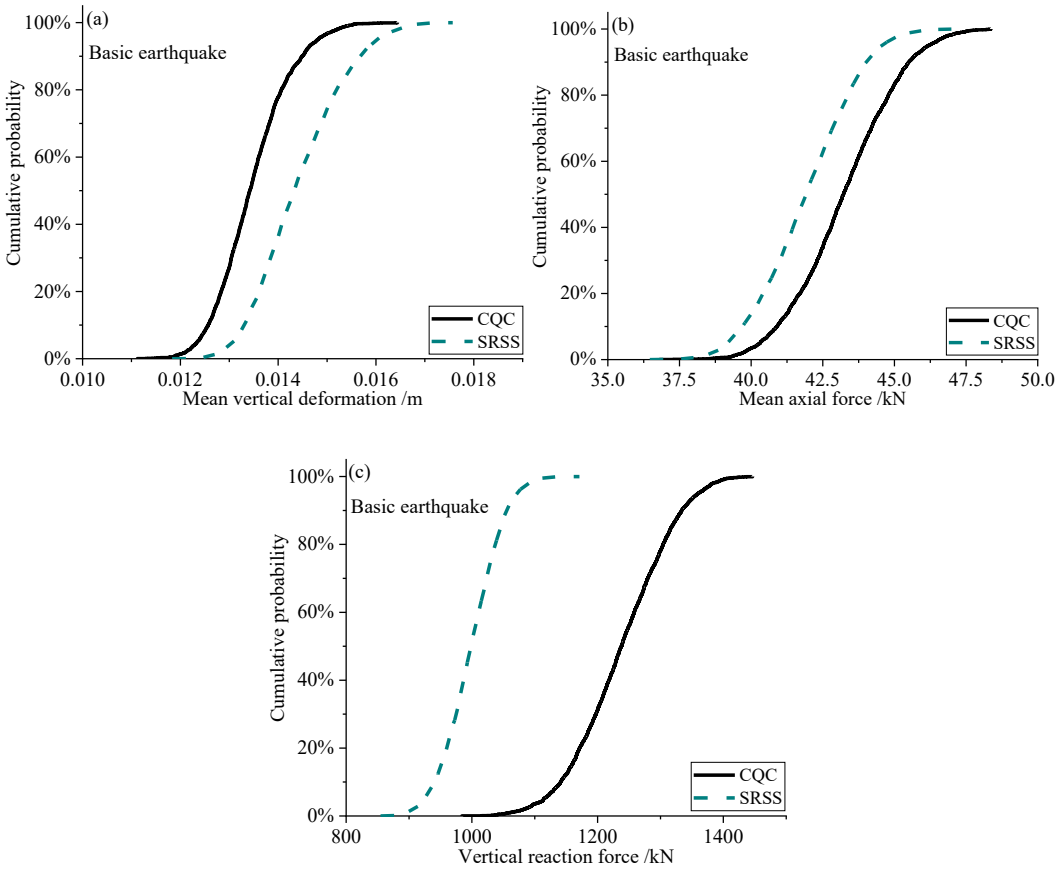

Fig. 23 Cumulative probability of the structural demands using different combination methods.

5. Effect of uncertain parameters on the structural demands

Uncertainty estimates play an important role in making decisions. Another important aspect of uncertainty analysis is the importance quantification of each uncertain parameter. In this study, the effects of each parameter on the maximum vertical structural deformation and axial force are analyzed. Here, each parameter is quantified based on 5000 sample structures. An evaluation indicator S_i of the i^{th} source is determined as,

$$S_i = \frac{Sd_{max} - Sd_{max,p}}{Sd_{max,p}} \tag{13}$$

where Sd_{max} is the maximum structural demand value (such as the maximum deformation in all nodes and the maximum axial force in all members) in the 5000 sample structures, and $Sd_{max,p}$ is the corresponding maximum structural demand value of the perfect dome.

Fig. 24 shows the evaluation indicator values under the basic earthquake level. According to the evaluation indicator values, it can be seen that these uncertain parameters have a greater influence on the deformation of the structure than on the axial force of the members. However, the geometric imperfections have the most significant effect on the deformation and axial force demands; for the deformation demand, the next factors are the cross-section, damping, load, and elastic modulus, while

for the axial force demand, the next factors are the damping, load, cross-section, and elastic modulus; it has been found that the effects of the different parameters on the different structural demands are not the same. In general, the low-level elastic modulus parameter has a small effect on the structural performance. In addition, according to Eq. (13) and Fig. 24, the results also reveal that the demand values of a dome with uncertain parameters are higher than those with deterministic parameters. Clearly, the existence of uncertain parameters results in the deterioration of the structural performance of the dome.

Unlike the THRA method [14], imperfections are the most important factor in a dome instead of the damping when using the RSA method to evaluate the structural seismic performance. In addition, the importance of the influence of these uncertain parameters on the structural performance is also different between the two methods. Therefore, researchers and structural engineers should comprehensively predict the impact of these uncertain parameters on the seismic performance of structures based on several methods.

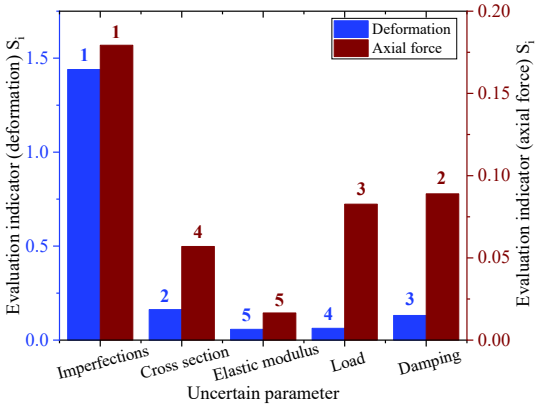

Fig. 24 Effect of uncertain parameters on the structural demands.

6. Conclusions

Uncertain analysis plays an important role in the PBEE framework. However, the probabilistic structural performance for large-scale single-layer lattice domes with multiple uncertainties has not been extensively investigated. The present study develops a probabilistic finite element code to evaluate the seismic performance of the dome using the RSA method under different earthquake intensity levels. Important uncertain parameters and their intervals are introduced in probability analysis. Based on a large number of sample structures, the structural demands are quantified, and the upper and lower bounds of the structural demands are given, presenting the uncertain characteristics. Compared with the perfect dome, it is found that in the imperfect dome, the statistical mean structural deformation and vertical reaction force values at the supports increase and the statistical mean axial forces in the members decrease; the standard deviations of the structural demands increase linearly with the earthquake intensity level, indicating that the uncertainty of the results increases as the earthquake intensity level increases. The effect of the modal combination method on the structural demands is discussed in this paper, indicating that in terms of estimating the structural demands of the single-layer lattice dome, there is a significant difference between the CQC method and the SRSS method. The effect of uncertain parameters on the structural demands is also discussed. The results show that each source has a different influence on important structural demands; in general, the geometric imperfections in the dome are the most important factor in the RSA method. Compared with THRA method, the developed method using the RSA is able to carry out the structural probabilistic analysis of complex large-scale structures with a higher sample precision.

Acknowledgements

The financial support from the National Key Research and Development Program of China (Grant No. 2018YFC1504304), the National Natural Science Foundation of China (Grant Nos. 51878433 and 51808380), and the Key Project of the Natural Science Foundation of Tianjin City (Grant No. 19JCZDJC39300) is acknowledged.

References

[1] Melchers RE. Human errors and structural reliability. Probabilistic Structural Mechanics Handbook. Springer US, 1995. DOI: 10.1007/978-1-4615-1771-9_10

[2] Ellingwood B. Design and construction error effects on structural reliability. Journal of Structural Engineering 1987; 113(2): 409-422. <https://doi.org/10.1061/(ASCE)0733-9445(1987)113:2(409)>

[3] DiMattia DG, Khan FI, et al. Determination of human error probabilities for offshore platform musters. Journal of Loss Prevention in the Process Industries 2005; 18(4-6): 488-501. DOI: 10.1016/j.jlp.2005.07.021

[4] Grierson D E, Xu L, et al. Progressive-failure analysis of buildings subjected to abnormal loading. Computer-Aided Civil and Infrastructure Engineering 2005; 20(3): 155-171. DOI: 10.1111/j.1467-8667.2005.00384.x

[5] Epaarachchi DC, Stewart MG. Human error and reliability of multistory reinforced-concrete building construction. Journal of performance of constructed facilities 2004; 18(1): 12-20. DOI: 10.1061/(ASCE)0887-3828(2004)18:1(12)

[6] Bonada J, Casafont M, et al. Selection of the initial geometrical imperfection in nonlinear FE analysis of cold-formed steel rack columns. Thin-Walled Structures 2012: 51: 99-111. DOI: 10.1016/j.tws.2011.10.003

[7] Sanayei M, Arya B, et al. Significance of modeling error in structural parameter estimation. Computer-Aided Civil and Infrastructure Engineering 2001; 16(1): 12-27. DOI: 10.1111/0885-9507.00210

[8] Johan de Haan. Human error in structural engineering: the design of a human reliability assessment method for stru ctural engineering. Master's thesis, Technical University Delft, Netherlands, 2012. <https://essay.utwente.nl/62118/1/HaanJde_20120913_openbaars.pdf>

[9] Fruhwald E, Serrano E, et al. Design of safe timber structures - how can we learn from structural failures in concr ete steel and timber? Technical report TVBK-3053, Lund Institute of Technology, Lund, Sweden, 2007. <https://portal.research.lu.se/ws/files/4514061/1553909.pdf>

[10] Liu HJ, Zhang W, Yuan H. Structural stability analysis of single-layer reticulated shells with stochastic imperfections. Engineering Structures 2016, 124: 473-479. DOI: 10.1016/j.engstruct.2016.06.046

[11] Fan F, Yan J, Cao Z. Elasto-plastic stability of single-layer reticulated domes with initial curvature of members. Thin-Wall Struct 2012; 60: 239-246. DOI: 10.1016/j.tws.2012.01.012

[12] Vryzidis I, Stefanou G, et al. Stochastic stability analysis of steel tubes with random initial imperfections. Finite Elem Anal Des 2013; 77: 31-39. DOI: 10.1016/j.finel.2013.09.002

[13] Bruno L, Sassone M, Venuti F. Effects of the equivalent geometric nodal imperfections on the stability of single layer grid shells. Engineering Structures 2016; 112: 184-199. DOI: 10.1016/j.engstruct.2016.01.017

[14] Zhang HD, Zhu XQ, Yao S. Nonlinear dynamic analysis method for large-scale single-layer lattice domes with uncertain-but-bounded parameters. Engineering Structures 2020; 203: 109780. DOI: 10.1016/j.engstruct.2019.109780

[15] Bradley BA. A critical examination of seismic response uncertainty analysis in earthquake engineering. Earthquake Engineering & Structural Dynamics 2013; 42(11): 1717-1729. DOI: 10.1002/eqe.2331

[16] Moller B, Graf W, et al. Uncertainty in damage assessment of structures and its numerical simulation. Computer-Aided Civil and Infrastructure Engineering 2001; 16(6): 375-383. DOI: 10.1111/0885-9507.00240

[17] Tsompanakis Y, Papadopoulos V, et al. Reliability analysis of structures under seismic loading. Fifth World Congress on Computational Mechanics, Vienna, Austria, July 7-12, 2002. <http://users.ntua.gr/nlagaros/files/rda.pdf>

[18] Naqvi T, Datta TK and Ramana GV. Reliability analysis of building frames for seismic forces. Transactions, SMiRT 16, Washington DC, August, 2001. <https://repository.lib.ncsu.edu/bitstream/handle/1840.20/30848/M1719.pdf?sequence=1>

[19] Basone F, Castaldo P, Cavaleri L, Di Trapani F. Response spectrum analysis of frame structures: reliability-based comparison between complete quadratic combination and damping-adjusted combination. Bulletin of Earthquake Engineering 2019; 17(5): 2687-2713. DOI: 10.1007/s10518-019-00559-7

[20] Moustafa A, Mahadevan S. Reliability analysis of uncertain structures using earthquake response spectra. Earthquake and Structures 2011; 3(2): 279-295. DOI: 10.12989/eas.2011.2.3.279

[21] JGJ 7-2010. Technical specification for space frame structures, Ministry of Housing and Urban-Rural Construction, Beijing, China, 2010. <http://www.gbstandards.org/GB_standard_english.asp?code=JGJ%207-2010&word=Technical%20specification%20for%20sp>

[22] Cai J, He S, Jiang ZR, et al. Investigation on maximum value of initial geometric imperfection in stability analysis of single layer reticulated shells. Journal of Building Structures 2015; 36(6): 86-92. DOI: 10.14006/j.jzjgxb.2015.06.011

[23] Liu XC, Zhang AL, Ge JQ, Wang L, Qi ZL. Study on the influence of construction deviation random distribution on the integral stability of suspend-dome. Journal of Building Structures 2007; 28(6): 76-82. <http://manu25.magtech.com.cn/Jwk3_jzjgxb/CN/>
[24] ASTM-A6/A6M-19, Standard Specification for General Requirements for Rolled Structural Steel Bars, Plates, Shapes, and Sheet Piling, ASTM International, West Conshohocken, PA, 2019, www.astm.org. DOI: 10.1520/A0006_A0006M-19
[25] Gendy BL, Hanna MT. Effect of geometric imperfections on the ultimate moment capacity of cold-formed sigma-shape sections. HBRC Journal 2017; 13(2): 163-170. <https://doi.org/10.1016/j.hbrcj.2015.04.006>
[26] de Paor C, Cronin K, Gleeson J, Kelliher D. Statistical characterisation and modelling of random geometric imperfections in cylindrical shells. Thin Walled Structure 2012; 58: 9-17. DOI: 10.1016/j.tws.2012.04.004
[27] Chen Z, Gandhi U, et al. Variation and consistency of Young's modulus in steel. Journal of Materials Processing Technology 2016; 227: 227-243. DOI: 10.1016/j.jmatprotec.2015.08.024
[28] JCSS. Probabilistic model code: Part II: Load models. Joint Committee on Structural Safety, 2001. <https://www.jcss-lc.org/jcss-probabilistic-model-code/>
[29] SEI/ASCE 7-02. ASCE 7: Minimum design loads for buildings and other structures. American Society of Civil Engineers, Reston, Virginia, 2013. < https://doi.org/10.1061/9780784406243>
[30] AS 1170.1-1989. Minimum design loads on Structures, Part 1: Dead and live loads and load combinations. Committee BD/6, Council of Standards Australia, 1989. <https://www.saiglobal.com/pdftemp/previews/osh/as/as1000/1100/11701.pdf>
[31] BS 6399. Loading for buildings: Part 1. Code of practice for dead and imposed loads. Technical Committee B/525, 1996. < https://crcrecruits.files.wordpress.com/2014/04/bs6399-1-1996-loading-for-buildings-dead-imposed-loads.pdf>
[32] Smith R, Willford M. Damping in tall buildings - uncertainties and solutions. 17th IABSE Congress: Creating and Renewing Urban Structures – Tall Building, Bridges and Infrastructure, Chicago, September 17-19, 2008. DOI: 10.2749/222137908796225618
[33] Kareem A, Sun WJ. Dynamic response of structures with uncertain damping. Engineering Structures 1990; 12(1): 2-8. < https://doi.org/10.1016/0141-0296(90)90032-N>
[34] Zhang HD, Liang X, Gao ZY and Zhu XQ. Seismic performance analysis of a large-scale single-layer lattice dome with a hybrid three-directional seismic isolation system. Engineering Structures 2020; 214: 110627. <https://doi.org/10.1016/j.engstruct.2020.110627>
[35] ABAQUS. ABAQUS theory manual and user's manual. Dassault Systèmes Simulia Corp., Providence, RI, USA, 2014. <http://ivt-abaqusdoc.ivt.ntnu.no:2080/texis/search/?query=wetting&submit.x=0&submit.y=0&group=bk&CDB=v6.14>
[36] Montgomery DC, Runger GC. Applied Statistics and Probability for Engineers. John Wiley & Sons, New Jersey, NJ, USA, 3rd edition, 2003. <http://www.um.edu.ar/math/montgomery.pdf>
[37] Yu RF, Zhou XY. Simplifications of CQC method and CCQC method. Earthquake Engineering and Engineering Vibration 2007; 6(1): 65-76. DOI: 10.1007/s11803-007-0640-7